

Hydron  
DESIGN & ENGINEERING  
PORTFOLIO



# OBJECTIVES & GENERAL RESEARCH

## WELCOME TO OUR JOURNEY

### TABLE OF CONTENTS

- Pg. 2 - Research & Development
- Pg. 3 - Research & Development
- Pg. 4 - Application of Computer Aided Analysis, Research & Development, 3D modelling
- Pg. 5 - Design Concepts, Application of Computer Aided Analysis, Research & Development, 3D modelling, Testing, Design Process Evaluation
- Pg. 6 - Design Concepts, Application of Computer Aided Analysis, Research & Development, 3D modelling, Testing, Design Process Evaluation
- Pg. 7 - Design Concepts, Application of Computer Aided Analysis, Research & Development, 3D modelling, Testing, Design Process Evaluation
- Pg. 8 - Testing, Design Process Evaluation
- Pg. 9 - 3D Modelling, Application of Computer Aided Analysis
- Pg. 10 - Use of CAM/CNC
- Pg. 11 - Other Manufacturing & Assembly

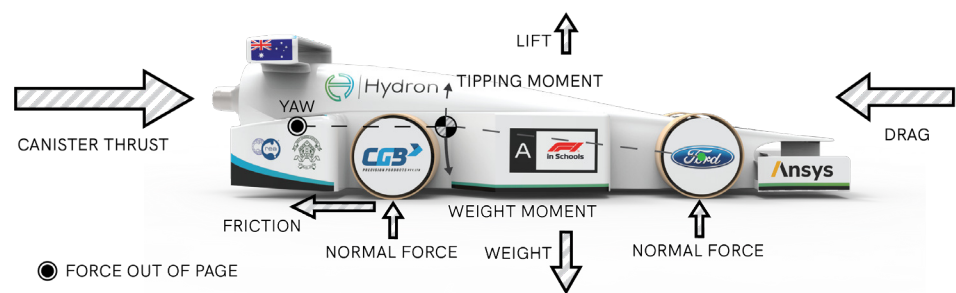
## INITIAL OBJECTIVES

Before beginning the development of our car, we established overarching objectives for the car to meet:

- » **Race Performance:** Achieve the best possible track times.
- » **Compliance:** Comply with all regulations.
- » **Durability:** Be durable enough to endure all races during the competition without need for repair.

These objectives can then be broken down into smaller, manageable design goals through research and testing.

### HYDRON WORLD FINALS 2022 FREE BODY DIAGRAM



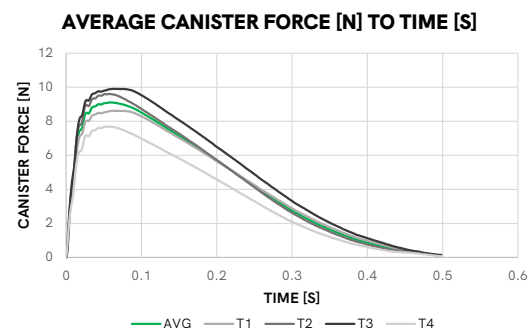
Free body diagram showing forces and moments on a Formula 1 in Schools car. Credit: Hydron

## LAUNCH EFFICIENCY

The energy conserved from initial launch is directly correlated to the track times of an F1 in Schools car. From reviewing race footage and directly measuring the force from a CO<sub>2</sub> canister, we found that the canister only applies thrust to the car for approximately 1/3 of the track length. In order to achieve the fastest track times, the limited energy from the launch phase must be conserved for as long as possible, with minimal losses.

## TRACK TESTING

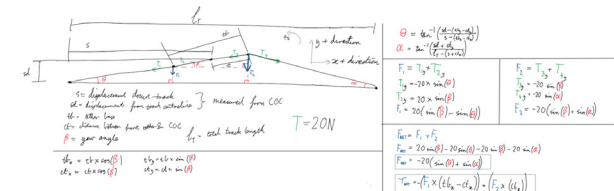
From testing the force output of CO<sub>2</sub> canisters, we found there to be a 20% error range when physically testing prototypes. For this reason, physically track testing prototypes for times was determined to be an inaccurate and inconsistent method of design evaluation. Instead, physical testing was conducted for individual factors which influence the car for a more controlled testing method.



Data from testing the force exerted by CO<sub>2</sub> canisters at launch. 4 trials and an average are included. Credit: Hydron

## MATHEMATICAL RACE MODEL

In order to more efficiently and accurately evaluate designs and iterations, we created a mathematical race model in Python. This included various factors that impact a race, such as tether line friction, yaw stability and tether line guide base. Physical testing was conducted to record the relationship between canister thrust and time, as well as wheel friction in relation to wheel speed.



Calculations deriving equations for net force and net moment from tether line tension. Credit: Hydron

In order to determine the race time of a car, thrust and friction forces as well as the mass of the car were used to calculate acceleration, and consequently velocity and position could be calculated.

Thrust is simply the force from the CO<sub>2</sub> canister, which was experimentally measured using force sensors with a time step of 0.001 seconds.

The total friction force of the car was more complex, as it was the sum of wheel friction, aerodynamic drag and tether line friction. Due to the dependence of tether line friction on sideways displacement as well as yaw angle, the simulation was expanded to track these variables along with all their interactions, even including yaw moments from off-centre canister punctures.

All of the relationships were integrated in over 900 lines of code, which then produced a track time given aerodynamic drag, car mass, length, wheel base and tether line guide height. The model also produced forwards displacement, velocity, acceleration, side displacement and yaw graphs, allowing more insightful analysis to be conducted.

A refine mode was also developed, which allowed us to investigate the effect of a single variable on race time. The output of the refine mode was a graph of race times for all values of the variable within a predefined range, allowing us to more easily optimise a prototype.



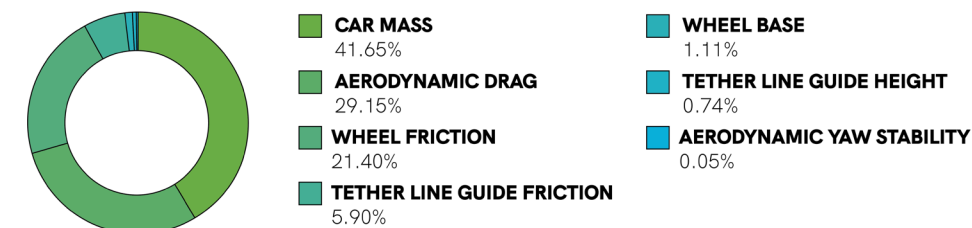
Left: Output data from race model. Right top: Race model refine mode output graph, illustrating direct correlation between increased car mass and increased lap times. Right bottom: Race model refine mode input. Credit: Hydron

## KEY FINDINGS

Before commencing car development, we used the race model to evaluate the importance of each variable used in the simulation. This allowed us to conduct more targeted research and development, using our resources and time most effectively in order to develop the fastest car possible.

In addition to providing weightings for each variable, the refine mode provided insight into trends in track time changes as a result of changed variables. For example, when changing the wheelbase, the increased aerodynamic drag from a longer wheelbase negated any track time improvements from beneficial wheel base changes.

## KEY PERFORMANCE INDICATORS



Key Performance Indicators weighted from race model data. Credit: Hydron

## THRUST EFFICIENCY

### TIPPING MOMENT

The tipping moment around the car's front axle can greatly impact the acceleration and maximum velocity of the car as it races. Caused by the centre of mass being typically unaligned with the canister thrust vector, an angular force about the front wheel is generated. This moment results in a multitude of problems, including an increased load on the front wheel, aerodynamic losses, as well as directional thrust losses. The tipping moment can be reduced by aligning the thrust vector closely with the centre of mass. In order to negate the effects of the tipping moment, the restoring moment resulting from the car weight can be increased by moving the centre of mass rearwards. In summary, the net tipping moment can be reduced by aligning the thrust vector with the thrust vector and having a rear positioned centre of mass. Therefore, we aim to align the centre of mass and canister thrust vector as closely as possible, vertically aligned within 5mm of the thrust vector, and as far rearwards as possible.

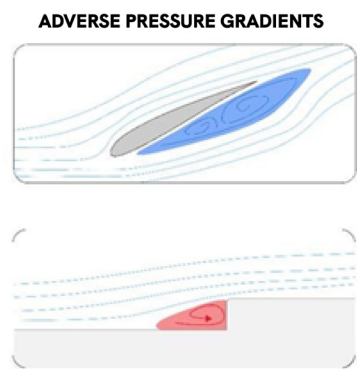
## INERTIA

Inertia is the resistance that an object has to a change in velocity, and is directly proportional to the mass of the object, while rotational inertia is quadratically increased based on mass and radius. Inertia is experienced during launch through both the rotational inertia of the wheels and inertia of the whole body. Thus, we could conclude that in order to reduce inertia, the **car needed to be as light as legally permitted** to reduce inertia and thus increase acceleration. This objective aligns with findings from our race model, where **41.65%** of overall car performance was dictated by car mass.

## AERODYNAMIC EFFICIENCY

### ADVERSE PRESSURE GRADIENTS

Adverse pressure gradients are regions of airflow recirculation, where air flows against the direction of the surrounding airflow. These are the primary cause for airflow separation on the car. Adverse pressure gradients behind a surface create a pocket of low pressure, resulting in increased drag.



\* Adverse Pressure Gradient Diagram. Credit: Hydron

Alternatively, this type of airflow is formed when a high-pressure region exists on a surface, possessing a flow direction opposite to its conventional surroundings. As stated in the name, adverse pressure gradients move in a direction 'adverse' to their surroundings, making them undesirable on an F1 in Schools car due to the inherent recirculation of airflow in the form of turbulent eddies, inducing pressure drag. Based on this information, **eliminating or reducing adverse pressure gradients** became a key aerodynamic objective in order to reduce drag.

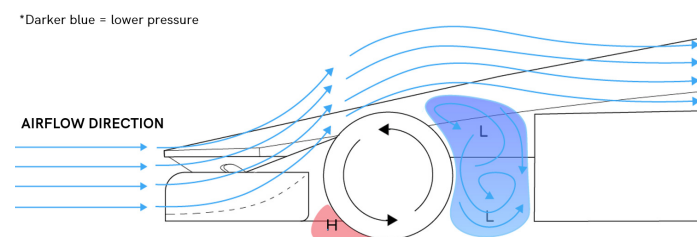
### WHEEL WAKE

Wheel wake is the result of the rotating surfaces of the wheel pulling airflow into a high-pressure region before being forced sideways, creating a large airflow separation region rearwards of the wheels. This has the overall effect of increasing drag and turbulence of the airflow rearwards of the wheel, reducing the aerodynamic efficiency of components rear of the front wheel.

### MAGNUS EFFECT

The Magnus effect is a phenomenon caused by the deflection of air from the counter-directional spin of the wheels on the top half of the front wheel, and the

directional spin of the wheels on the bottom half of the front wheel in relation to the direction of airflow. This creates a large low-pressure zone above the centre of mass, as well as a high-pressure region at the bottom of the wheel, resulting in an overall increase in drag and lift.



\* Magnus effect and wheel wake diagram. Credit: Hydron

Due to both the wheel wake and Magnus effect, the drag produced by the front wheel faces was found to severely impact overall drag values. When isolating this drag force, it accounted for 54.05% of the total drag of the car. As a result, we identified one of our primary aerodynamic objectives to be **reducing airflow collision with the rotating surfaces of the wheels**.

## SUMMARY OF KEY DESIGN OBJECTIVES

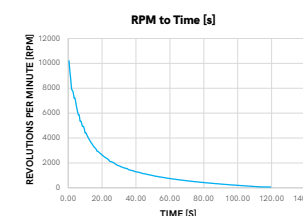
As a result of our research and testing, we compiled the following list of overall key design objectives by order of priority:

- » **Car mass:** The car should be as close to the 50g limit as possible.
- » **Durability:** The car must be able to withstand 10 races without breakage.
- » **Compliance:** The car should comply with all regulations.
- » **Aerodynamics:** Reduce or eliminate adverse pressure gradients.
  - » Redirect airflow away from rotating wheel surfaces.
  - » Achieve a drag value as low as possible given technical restrictions.
- » **Tipping moment:** The centre of mass should be vertically aligned to be within 5 mm of the canister thrust vector to reduce the effects of tipping moment.

## BEARING RESEARCH

In order to select the best bearings for our car, we tested various bearing types and many different lubricant options, along with the effects of burnishing. In this testing, a specialised machine was utilised to reduce human error in measurement, and to automate data collection. Using the motor, the machine spins each wheel to 7,000 RPM for any burnishing revolutions, and

then spins it at 12,000 RPM before releasing the arm and recording spin time. The machine collects data through a laser diode opposite a photodiode, which tracks the passing of spokes, from which the rotation speed can be derived.

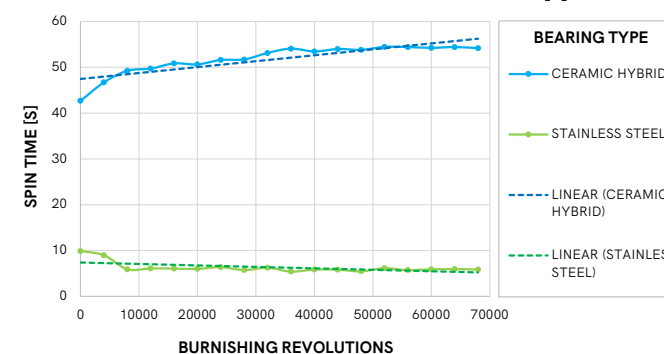


\* Left: Bearing test rig in operation. Right: RPM to time data from the bearing test rig. Credit: Hydron

## BURNISHING INVESTIGATION

We first investigated different types of bearings and their spin times in relation to burnishing revolutions. Both stainless steel and hybrid ceramic bearings were tested, from 0 to 68,000 burnishing revolutions. The hybrid ceramic bearing performed consistently better than the steel bearing at any amount of burnishing revolutions, with a best time of 54.43 seconds in comparison to steel's best of 9.90 seconds. Hybrid ceramic bearings also exhibited a positive correlation between spin time and burnishing revolutions, with a 21.53% increase in spin time over 68,000 revolutions, from 42.71 seconds to 54.43 seconds. As a result, **we selected a hybrid ceramic bearing, SMR73C-20S #7 LD**, as our bearing for the car.

### BURNISHING REVOLUTIONS TO BEARINGS SPIN TIME [S]



\* Burnishing revolutions to bearing spin time [s] data from the bearing test rig. Credit: Hydron

## LUBRICATION & SEALS INVESTIGATION

The next step was to investigate lubrication and the effects of removing seals. We hypothesised that the removal of seals would initially result in longer spin times due to lower friction, but that over time contamination would build up, so we focused on testing this in addition to lubricant types.

BEARING CONDITION	SPIN TIME [S]			
	TRIAL 1	TRIAL 2	TRIAL 3	AVERAGE
SEALS	119.63	116.74	115.14	117.17
SEALS REMOVED	114.73	115.35	114.83	114.97
EXPOSED TO OPEN AIR 7 DAYS	66.37	72.82	80.42	73.20
EXPOSED TO SAWDUST	33.50	34.62	34.91	34.34

BEARING LUBRICANT	SPIN TIME [S]			
	TRIAL 1	TRIAL 2	TRIAL 3	AVERAGE
FACTORY LUBRICANT	119.63	116.74	115.14	117.17
KEROSENE 1 MIN SOAK	85.78	90.94	92.37	89.70
LIGHT MACHINE OIL	27.58	28.38	27.56	27.84
ISOPROPYL 1 MIN SOAK	112.51	104.30	102.02	106.28
ISOPROPYL 12 HR SOAK	126.66	119.38	123.95	123.33
ISOPROPYL 24 HR SOAK	92.02	87.01	85.28	88.10
ISOPROPYL 7 DAY SOAK	102.96	97.92	94.61	98.50

\* Spin time data for a variety of lubricant and seal configurations. Credit: Hydron

As according to our research, SMR73C-20S #7 LD hybrid ceramic bearings with **factory lubrication and seals resulted in the longest spin times and thus lowest friction**, so this bearing configuration was selected. We also noted that removal of seals and exposure to dust, even if indirectly, resulted in vastly decreased spin times, so **a clean environment while handling bearings was prioritised**.

## APPLICATION TO RACE MODEL

Using the data collected during testing, we were able to derive the bearing friction at different accelerations, which we then applied to our race model. To derive this function, the rpm to time approximate function was differentiated, and then the angular equivalent of Newton's Second Law was applied to this function, which after further rearrangement produced bearing friction as a function of angular acceleration.

$$F_f = \frac{\pi \left( \delta \left( \frac{95000}{(t+8.5)} - 700 \right) \right)}{14.2 \times 10^{-3}} * 402.583 * 10^{-9}, t \in [0, 119]$$

$$Inverse = \frac{0.5(178100 - 17t)}{t + 700}$$

$$F_f = \frac{\pi \left( \frac{\delta f(f^{-1}(rpm))}{\delta t} \right) * I_{wheel}}{r}$$

$$f(t) = \frac{95000}{(t+8.5)} - 700 = \text{time to rpm function}$$

$I_{wheel}$  = moment of inertia of wheel  
 $r$  = radius

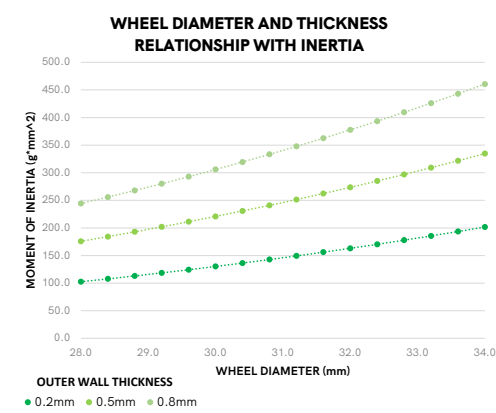
## MOMENT OF INERTIA

Moment of inertia is a body's resistance to angular acceleration. When the car accelerates after launch, the wheels must rapidly accelerate to over 1400 rad/s in order to allow the car to reach top speed as quickly as possible. For the wheels to accelerate so quickly, the least amount of resistance to angular acceleration is desirable, meaning that **we aimed to minimise the moment of inertia of the wheels**.

## WHEEL RADIUS & THICKNESS

Mass and mass distribution determine the moment of inertia of solids, so we investigated the effects of radius and thickness of track contact surface on the moment of inertia of our wheels. Moment of inertia was recorded directly from Fusion 360, over the range of legal dimensions. Fusion 360 was chosen for the application of wheel development as it allowed rapid and simple FEA testing and moment of inertia tools.

Increases in both outer wall thickness and wheel diameter resulted in increased moment of inertia, with wheel diameter affecting moment of inertia in a quadratic relationship. For this reason, we designed our wheels to be as close to the minimum legal wheel radius, while allowing for tolerance, and aimed to **have the thinnest outer walls while satisfying our structural goals.**



✖ Wheel diameter and thickness relationship with moment of inertia. Credit: Hydron

## YIELD STRENGTH

The yield strength is the stress at which deformation changes from elastic deformation to plastic deformation, or a permanent change in the material's size and/or shape occurs. As our wheels needed to be reusable, we aimed to limit all deformation to elastic deformation, and thus keep all stresses below the yield strength of the chosen materials. We decided to aim for a **peak stress of 60% of the yield strength**, allowing a safety factor of approximately 9:5. The force at which wheels were tested was 50N, 10 times higher than the maximum force experienced on the track during deceleration, but an approximation of the highest force which the wheels would need to withstand during manufacturing and handling.

## DEFORMATION

Rolling resistance is due to deformation of wheels in contact with the ground surface, and as wheel deformation increases, so does rolling resistance. We aimed to reduce the losses in the wheel system, and so **stiff wheels with low deformation was a key goal.**

## TRACK TESTING

While moment of inertia can be reduced through removing material furthest from the axle, this decreases the stiffness of the wheel, meaning it was necessary to model this trade-off. In order to do this, we conducted physical testing of both stiff and low moment of inertia wheels. We controlled variables such as material (Nylon-12) and the total mass of the car by ballasting both to 50g, in order to improve the validity of the experiment. The 1.28g wheels, which were more rigid but had higher moments of inertia than the 0.80g wheels consistently outperformed the 0.80g wheels, with an average time of 1.182 seconds in comparison to 1.185 seconds.

WHEEL TYPE	TRACK TIME [S]			
	TRIAL 1	TRIAL 2	TRIAL 3	AVERAGE
LOW MOMENT OF INERTIA FLEXIBLE	1.185	1.150	1.221	1.185
HIGH MOMENT OF INERTIA RIGID	1.196	1.183	1.167	1.182

✖ Race times from track testing of different wheel rigidities. Credit: Hydron

Following this experiment, we ensured that **deformation of wheels was kept to a maximum of 0.25mm**, and then optimised wheels to have the lowest moment of inertia while maintaining this condition.

## SUMMARY OF WHEEL DESIGN OBJECTIVES

As a result of our research and testing, we compiled the following list of wheel design objectives in order of priority:

- » **Durability:** The wheels must have a peak stress of 60% of the yield strength of the selected material at 50N.
- » **Compliance:** The wheels must comply with all wheel regulations.
- » **Manufacturability:** The wheels must be manufacturable.
- » **Stiffness:** The wheels should have a maximum deformation of 0.25mm at 50N.
- » **Moment of Inertia:** The wheels should have a moment of inertia that is as low as possible.

## MATERIAL SELECTION

During material research we identified stiffness, strength, density, and manufacturability as relevant material properties, as they all affected how well the wheels satisfied our goals. We compared the following materials, aiming for high yield strength and Young's Modulus (stiffness), low density and manufacturing which allowed us to produce the best wheel.

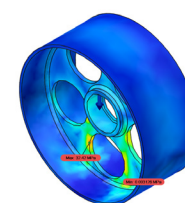
MATERIAL	TENSILE STRENGTH (MPa)	FLEXURAL STRENGTH (MPa)	YOUNG'S MODULUS (MPa)	DENSITY (g/cm <sup>3</sup> )	MANUFACTURING METHOD
Nylon 12	38.5-46	61-67	1138-1282	1.01	SLS 3D Printing
Accura Xtreme	38-44	52-71	1790-1980	1.19	SLA 3D Printing
Ketron PEEK 1000	110	172	4340	1.31	CNC Machining
Accura Bluestone	66-68	124-154	7600-11700	1.78	SLA 3D Printing
Ertalyte tx	76	96	3300	1.44	CNC Machining

✖ Material properties comparison table, used in order to select the optimal material. Credit: Hydron

As a result of our research, we selected Ketron PEEK 1000, as it had the best material properties, and was also able to be CNC turned, which would result in extremely circular and concentric wheels. Our **maximum permissible stress was therefore 60% of 110MPa, or 66 Mpa.**

## DESIGNS & EVALUATIONS

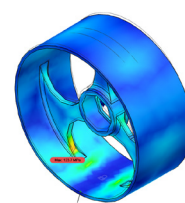
### 5 HOLE DESIGN



**Peak Stress:** 32.42 MPa  
**Maximum Deformation:**  $1.06 \times 10^{-4}$  m  
**Moment of Inertia:** 168.86 gmm<sup>2</sup>

This design was a regulation compliant adaptation of our National Finals wheel, with holes drilled through a thin central wall for a low moment of inertia with simple and fast manufacturing. While the peak stress and maximum deformation were both well within our targets, no more material could be removed while retaining a manufacturable wheel. The minimum moment of inertia for our manufacturable iterations proved higher than other designs, and therefore this design was not pursued further.

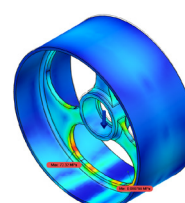
### 3 SPOKE DESIGN



**Peak Stress:** 123.7 MPa  
**Maximum Deformation:**  $3.92 \times 10^{-4}$  m  
**Moment of Inertia:** 159.70 gmm<sup>2</sup>

This design was based on our previous research showing that an odd number of spokes resulted in more even deformation around the wheel. While having a lower moment of inertia than the 5 hole design, the large sections of unsupported rolling surface resulted in large stress and deformation. This meant that the design failed to meet our criteria, and thus was not implemented as our final design.

### 3 SPOKE WITH RIB DESIGN

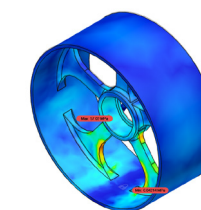


**Peak Stress:** 73.32 MPa  
**Maximum Deformation:**  $3.92 \times 10^{-4}$  m  
**Moment of Inertia:** 165.77 gmm<sup>2</sup>

This design was intended to improve on the 3 spoke design's weaknesses,

and incorporated a rib running along the inside of the rolling surface to reinforce the wheel and distribute force better. The rib brought the peak stress closer to being within our goals, but both stress and deformation were still too high. The addition of the rib also increased the moment of inertia by 6.07 gmm<sup>2</sup>, only slightly better than the 5 hole design. As there were still high amounts of deformation and only small improvements to the moment of inertia, this design was not chosen.

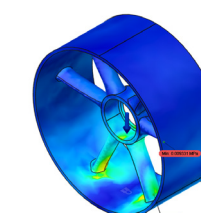
## 5 SPOKE DESIGN



**Peak Stress:** 57.02 MPa  
**Maximum Deformation:**  $1.97 \times 10^{-4}$  m  
**Moment of Inertia:** 156.85 gmm<sup>2</sup>

This design was based on the 3 spoke design with the goal of reducing the areas of displacement by adding additional spokes in the large gaps. This meant that stress was also distributed more evenly throughout the wheel, and both peak stress and displacement were within our goals. This wheel had the lowest moment of inertia of all the wheel designs, and met all of our wheel objectives. Hence, this design was most suitable for the final design.

## TOPOLOGICAL OPTIMISATION



**Peak Stress:** 84.05 MPa  
**Maximum Deformation:**  $5.34 \times 10^{-4}$  m  
**Moment of Inertia:** 163.41 gmm<sup>2</sup>

This concept was created using a vastly different approach to the other designs. Using Fusion 360's Generative Design workbench, a shape optimisation was run. The result was a wheel which performed extremely well in its strongest orientation with peak stress of only 33.51 MPa. In other orientations, the wheel had much poorer performance, with both deformation and stress outside of our acceptable range. Due to the curved and irregular organic shape of the spokes, it would be impossible to CNC machine such a wheel out of PEEK.

## FINAL WHEEL SELECTION

From testing our range of design concepts and comparing results with our objectives, we identified our 5 spoke wheel as the best performing design. It successfully met all of our criteria, in both front and rear wheel width configurations, and provided the lowest moment of inertia of all our wheels. As a result we selected the 5 spoke wheel design for our car.

## PRIOR DEVELOPMENT & TESTING PRECISION

Rather than viewing the World Finals as a separate design process, we considered all findings and development of the car from previous competitions. This enabled us to continue to develop and build upon prior designs. Computer-based analysis techniques were conducted with the intention of changing only one element or factor between tests. This enabled our team to definitively determine the impact on aerodynamics with respect to each change to the design.

In order to determine how current results compared to our findings from prior competitions, the same car was tested with the same flow and simulation condition, examining the reproducibility of drag results between ANSYS Discovery Aim, which was utilised until the 2020/2021 National Finals, and ANSYS Fluent, which was used as our CFD software for the World Finals.

The results were as follows:

**Fluent:** 0.22693 [N]

**Discovery Aim:** 0.21112 [N]

Due to the high level of reproducibility between the two types of CFD software, with the mean drag and lift value differing by a maximum of 0.00790N, our team was able to confidently rely on previous findings as the basis for further development of our car in preparation for the World Finals.

## NATIONAL FINALS CAR

Before developing new prototypes, an overall analysis and evaluation of our most recent car provided our team with valuable insight as to the key improvement actions which must be undertaken in car development for the World Finals. Comparing our findings in CFD to that of physical wind tunnel testing, we were able to affirm the accuracy of our testing to that of airflow behavior for a physical model.



Physical wind tunnel used to measure drag force of our National Finals car. Credit: Hydron

**Physical Model Drag:** 0.19N

**CFD Theoretical Drag:** 0.21N

## THEORETICAL VS PHYSICAL DRAG

From comparing the theoretical drag of the car to that of the drag of the car when physically tested, it was found that the CFD simulations would yield slightly higher drag forces than in reality, differing by 0.02N. However, such a difference can be considered negligible when the lack of

rotating wheels in the physical wind tunnel is considered.

## DESIGN EVALUATION

The convex-concave nosecone is effective in coercing airflow away from the front wheels on the main body, however the large fillet on the edges of the nosecone reduced effectiveness of the nosecone design, enabling airflow to roll over the edge and into the front wheel. The G0 continuity (see page 9) between the nosecone and main body resulted in surfaces which were slightly sharp in the CAD model, which could result in errors while attempting to create fillets or other geometry near the connection. While a sturdy design, the large leading edge which wraps around to include the channel walls resulted in initial boundary layer separation upon airflow collision with these edges.

## IMPROVEMENT ACTIONS

- Further exaggerate the convex-concave nosecone geometry and reduce fillet sizes to minimise rollover from nosecone onto the front wheel.
- Ensure g1 continuity between nosecone and body for reducing errors in the CAD model.

## IMPLEMENTATION WITH WORLDS REGULATIONS

With the introduction of a new set of regulations, large portions of the car design had to be rethought, making it difficult to adapt our Nationals car design without needing to entirely redesign central components. The new wheel regulations drastically affected the overall design of the car, requiring higher side components and new parameters for all side components. As a result, rather than simply adapting our Nationals car for the World Finals, development of new prototypes inspired by and improving upon the features of our Nationals car and driven by previous findings were developed.

## DESIGN PROCESS

Beginning with the individual development of prototypes, each engineer simultaneously designed their own prototype separately, labelled as A,B,C and D. This design process was implemented with the intent to promote a variety of design approaches and innovations. After analysing each prototype for their beneficial features, one prototype with combined individual components was created.

## PROTOTYPE A



## CONCEPT AIM

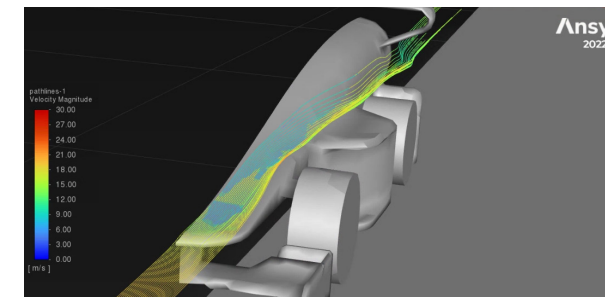
The nosecone features our convex-concave features initially, before transitioning to two airflow contours to redirect air to the top of the side components, re-energising the airflow behind the front wheel and thus reducing the size of the adverse low pressure gradient. This prototype focussed on the leading surfaces of the car directing airflow towards the centre, while at the side pods redirecting air outwards to the side components to reduce the adverse pressure gradient behind the front wheels.

## DESIGN ANALYSIS

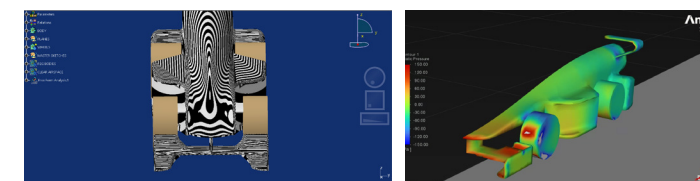
Drag: 0.3027N

Lift: -0.1281N

Math Model Race Time: 1.081 s



PROTOTYPE-A Streamlines velocity magnitude analysis [0,30m/s]. Credit: Hydron



Left: PROTOTYPE-A Isophotes Mapping Analysis - The body and nosecone are seamlessly joined together to smoothly coerce airflow outwards to side components. Right: PROTOTYPE-A Static pressure contour analysis [-150,150Pa]. Credit: Hydron

The nosecone was effective in redirecting airflow away from the front wheels, however the centre channel which did not have any walls to separate the front wheels resulted in wheel wake not only affecting the side components but also the airflow in the centre channel of the car.

## DESIGN EVALUATION

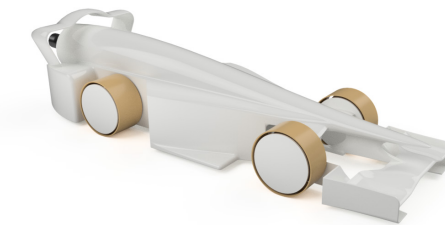
While the innovation had its intended effect, the open-channel design for the front of the car resulted in additional drag for the car which made the prototype perform worse overall. The front wing being supported by one structural piece was undesirable, as it means there could be issues with breakage during racing.

## IMPROVEMENT ACTIONS

- Create a physical barrier between the front wheel and central airflow channel to prevent wheel wake into the central channel.

- Increase connection points of the front wing to the body for stability.

## PROTOTYPE B



## CONCEPT AIM

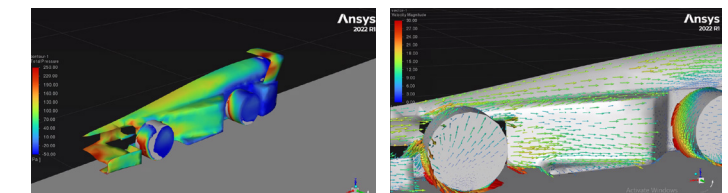
This prototype features a gradually curved streamlined body shape, with the intent to create a more even pressure distribution, therefore minimising pressure drag. The design also features a graduated transition between the main body and side pods, unifying the different components with minimal airflow disturbance. The front wing of this design was also connected to the rest of the car at an additional two points in order to increase strength.

## DESIGN ANALYSIS

Drag: 0.3088N

Lift: -0.0611N

Math Model Race Time: 1.083 s



Left: PROTOTYPE-B Pressure distribution of an early iteration. Right: PROTOTYPE-B Vector analysis over side components, demonstrating success of graduated transition geometry. Credit: Hydron

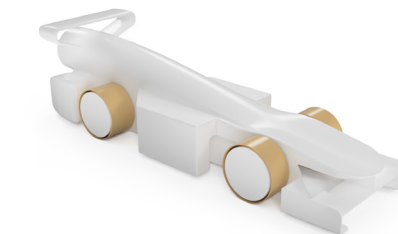
## DESIGN EVALUATION

After 4 iterations of the body shape, an even pressure distribution over the body was successfully achieved, albeit with low energy airflow at the rear of the body. Whilst the tangent support structure for the side pods disturbed the airflow minimally locally, further downstream the pressure difference between faces of the side pods caused rollover on the edge of the side pod.

## IMPROVEMENT ACTIONS

- Isolate central channel from front wheels
- Strengthen support of front wing structure

## PROTOTYPE C

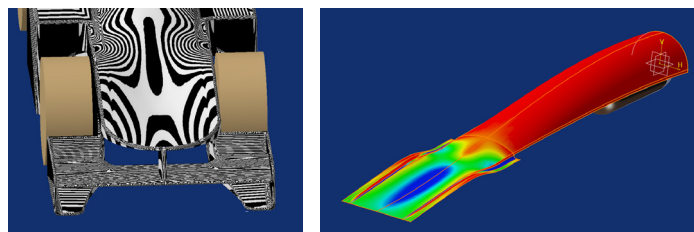


### CONCEPT AIM

The body is shaped to fully cover the side of the front wheels, accentuating the concave-convex nosecone design for a greater effect of redirecting airflow away from the front wheels. The side pods have an inlet positioned to redirect airflow from the centre channel out towards the side components, re-energising airflow and reducing the pressure drag from the low pressure zone behind the side pod.

### ANALYSIS

Drag: 0.2931 N  
Lift: -0.1443 N  
Math Model Race Time: 1.078 s



✦ Left: PROTOTYPE-C Isophotes Mapping Analysis - The body and nosecone smoothly joined, with accentuated concave section foremost. Right: PROTOTYPE-C Surface Curvature Analysis - The body and nosecone are seamlessly joined together, with the varied curvature of the nosecone becoming smoother towards the rear of the car. Credit: Hydron

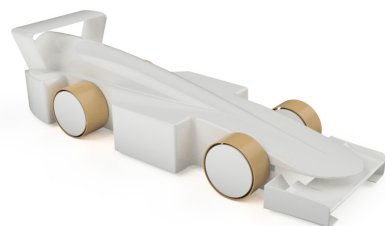
### EVALUATION

While the heightened nosecone was effective in minimising the effects of the front wheel wake on airflow over the body, it also increased the pressure on the nosecone and created a low pressure zone behind the heightened sides. The side pod inlet proved ineffective in aiding airflow attachment to the side components, rather resulting in more drag as the air collided with the rotating face of the rear wheel.

### IMPROVEMENT ACTIONS

- Reduce height of nosecone to reduce pressure build-up on the nosecone and to reduce weight at the front of the car
- Remove inlets from side pods to isolate central channel from turbulence of front wheel wake
- Taper side pods slightly inwards and apply larger fillets to prevent turbulence that is resultant of airflow collision with the front edges

### PROTOTYPE D



### IDEA

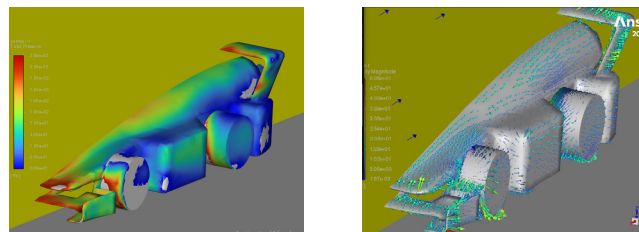
The composite body shape with two separate surfaces is shaped to cleanly direct airflow over the side pods, encouraging flow attachment over side components. This also allows for a more gradual curve over the canister chamber. Retaining the nosecone innovation of our Nationals car, it is slightly concave at its centre, directing flow away from the wheels of the car, before the rest of the body directs it outboard downstream.

### ANALYSIS

Drag: 0.2868 N  
Lift: -0.1461 N  
Math Model Race Time: 1.076 s



✦ PROTOTYPE-D Isophotes Mapping Analysis - Nosecone and side pod top surfaces are tangential, encouraging airflow over side pods. Credit: Hydron



✦ Left: PROTOTYPE-D Pressure distribution analysis - High pressure regions on the nose and extending along the body. Low pressure regions along side of body towards the rear. Right: PROTOTYPE-D Vector Analysis - Low velocity zones towards rear of the body and over side pod surface indicate poor flow attachment. Credit: Hydron

### EVALUATION

While the slight concavity of the nosecone successfully resulted in airflow moving inboard of the front wheels, the rear portion of the composite body had poor pressure distribution. The nose of the car did not direct flow onto the side pods as intended, with poor airflow attachment on the side pods. In order for the nose to smoothly join with the side pod surfaces, a steeper than usual guide curve was required, resulting in higher pressure at the front of the car.

### IMPROVEMENT ACTIONS

- Ensure that main body does not negatively interfere with airflow over side pods through trialling a similar design using one surface.

- Utilise rear wing and wing support structures to assist in reenergising airflow at the rear of the car.
- Adjust the nosecone to have a more shallow curve.

### COMBINED PROTOTYPE



After prototypes A, B, C and D were designed, the key improvement actions were then compiled and were applied to a single combined prototype. The combined prototype took the convex-concave nosecone from our National Finals car, while implementing continuous channel walls along the body for uninterrupted airflow through the central channel. The side pods were slightly tapered to account for the wheels being positioned slightly inwards.

### ITERATIVE COMPONENT DEVELOPMENT

After general prototypes were developed and the combined prototype was made, iterative development was then conducted. This involved small changes to specific components in the design to incrementally determine what parameters, shape and configuration resulted in the lowest drag force possible. Components were developed sequentially from the front rearwards in correspondence with the airflow direction. This ensured changes to a design rearwards was not impacted by changes to features in front.

### FRONT WING

#### TWISTED FRONT WING

Having a neutral angle of attack on the front wing, whilst easiest to ensure regulation compliance, has the downside of redirecting less airflow over the front wheel, resulting in more collision. Therefore a twisted front wing, like that found on both the front wing and rear wing of F1 cars was proposed as a solution as an additional front wing element to efficiently redirect airflow over the front wheel by smoothly changing the angle of attack on a wing.

Flat: 0.2760 N

Twisted: 0.2591 N

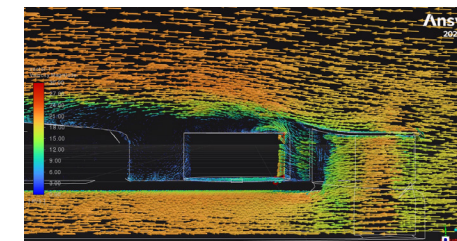
### EVALUATION

Compared to a neutral wing, a twisted front wing was found to reduce drag by 0.0169[N] with the only downside being slight manufacturing and scrutineering difficulties, but such downsides were deemed negligible

in comparison to the overall gains and was therefore implemented in our design.

### SWEPT ENDPLATE

Any angled wing will have a high pressure region and a low pressure region on either side of the aerofoil. Inspired by the endplates found on F1 cars, endplates prevent rollover between these two pressure regions, increasing the efficiency of the wing and minimising vortex generation on the front wing. The sweep on the endplate aids in redirecting air away from the front wheel in a horizontal direction rather than vertically.



✦ Vector Analysis of front wing endplate, illustrating airflow deflected around the side of the wheel. Credit: Hydron

### EVALUATION

The endplate not only reduced drag on the car, but also structurally reinforced the front wing and it was therefore implemented in the design.

### VORTEX GENERATORS

As found on F1 cars, vortex generators are a device which, through the rollover of air from the high pressure region to the low pressure region of a profile, creates a vortex that when implemented on the front wing can aid in retaining airflow adhesion to side components. This would be especially useful for the rear of our car, where airflow separates from the car surfaces and a low-pressure recirculation zone is formed, inducing drag.

VORTEX GENERATOR DESIGN (mm)	VORTEX SIZE	INDIVIDUAL DRAG [N]	DRAG OFFSET WHEN APPLIED [N]
1	LARGE	0.021	+0.11
2	MEDIUM	0.022	+0.04
3	SMALL	0.018	+0.02
4	LARGE	0.019	+0.06
5	MEDIUM	0.017	+0.07
6	SMALL	0.015	+0.05

### EVALUATION

While a vortex may be applicable in F1 cars, the nature of a vortex created on the front wing, subject to the turbulent airflow from the wheel wake, is unpredictable. Since control surfaces like those found on an F1 bargeboard cannot be implemented 15mm rear of the front wheel, a vortex generator was found to be an ineffective addition to the car. When implemented into a design, there was an overall increase in drag, therefore we decided against implementing vortex generators in our car design. Rather, we identified the reduction of wingtip vortices on the front wing as a key improvement action for the front wing.

## MULTI-ELEMENT WINGS

A configuration with the classified front wing on top with an additional element underneath to direct as much air as possible over the front wheel was found to be most optimal. The element underneath is responsible for the majority of airflow deflection, while the legal front wing aids in additional airflow redirection. These two aerodynamic elements result in the most efficient redirection of airflow away from the front wheel, without sacrificing drag from airflow collision with additional elements.

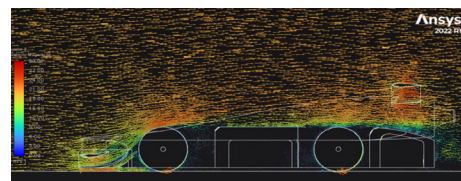
## FRONT WING EVALUATION

The front wing was extensively tested to determine the best possible arrangement and geometry. A double element wing design was implemented in our final design, with a twisted wing which aids in deflecting airflow over the front wheels.

## SIDE PODS

### FLAT SIDE PODS

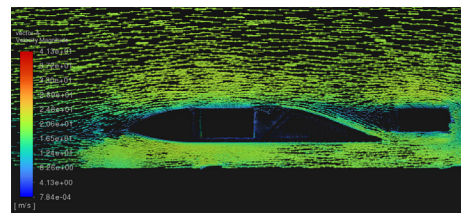
The front wing was extensively tested to determine the best possible arrangement and geometry. A double element wing design was implemented in our final design, with a twisted wing which aids in deflecting airflow over the front wheels.



✦ Vector Analysis - Airflow reconnection over the top surface of flat sidepods. Credit: Hydron

### TAPERED SIDE PODS

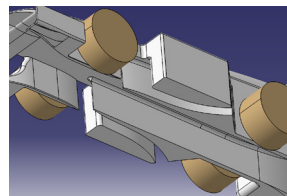
Tapered side pods can be used to redirect airflow around the rear wheel, and allow for a less abrupt transition from airflow redirected by the front wing and front wheel wake. They were also used to minimise the low pressure wake of the front wheels, in order to reduce the pressure drag of the car.



✦ Vector Analysis - minimised region of airflow disconnection behind front wheel. Credit: Hydron

### INLETS

Side pods with an inlet can be used to redirect airflow between the central channel and the side components of the car, which can be useful to re-energize airflow in adverse pressure zones.



SIDE POD DESIGN	MANUFACTURING DIFFICULTY	DRAG [N]	LIFT [N]
FLAT	SIMPLE	0.2111	-0.1075
INDENT	DIFFICULT	0.2178	-0.1052
INLET	NORMAL	0.2163	-0.1180
TAPERED	NORMAL	0.2149	-0.1460

## EVALUATION

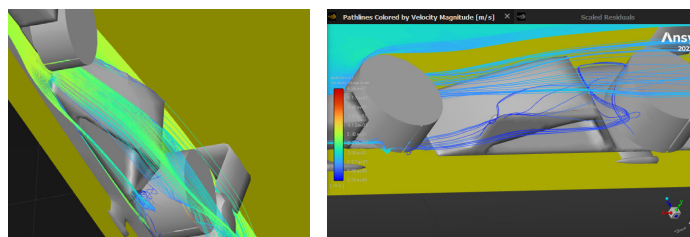
While the inlet design did re-energize airflow in the adverse pressure zones present in front of the rear wheels, its drag values were still higher than most other designs. The indented design, while able to prevent turbulent airflow from bleeding over to the side faces of the side pods, ultimately was not implemented due to its difficulty to manufacture, resulting in large tolerances which could negate any benefits of the design. The tapered design, while effective in redirecting airflow from the centre channel outwards to side components and reducing the adverse pressure zone behind the front wheel, resulted in laminar airflow from the centre channel being influenced by the turbulent air of the front wheel. As a result, there was increased drag and was therefore not implemented as our side pod design. The flat side pod, the simplest of all the side pod designs, was chosen for its ease of manufacturability, and low drag value.

## IMPROVEMENT ACTIONS

- Use variable fillets on the side pod edges to allow for a more gradual transition between components on a flat side pod.

## SIDE POD PLATES

If the side pod is angled, the higher pressure on the angled face can result in airflow rolling over the top and underneath the side pod. As a potential solution to this, side pod plates were implemented which act as a physical barrier to prevent such rollover from occurring.



✦ Left: Pathlines Analysis - Airflow underneath standard tapered side pods. Right: Pathlines Analysis - Reduced airflow under side pods following the addition of side pod plate. Credit: Hydron

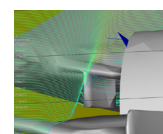
## SIDE POD PLATES EVALUATION

Side pod plates are an effective addition to a tapered side pod, however, the drawbacks of implementing a tapered side pod outweigh the improvements in drag that adding an endplate would add. As a potential improvement to a flat side pod, a plate or thicker wall on the front face could prevent rollover underneath the side pod.

SIDE POD ENDPLATE CONFIG.	MANUFACTURING DIFFICULTY	DRAG [N]	LIFT [N]
NONE	SIMPLE	0.2507	-0.1875
BOTTOM	DIFFICULT	0.2521	-0.1952
TOP	NORMAL	0.2576	-0.1830
BOTH	NORMAL	0.2597	-0.1879

## SIDE POD BARGEBOARD

Another problem with the tapered side pod design was that airflow that was diverted inboard from the front wheels was not following the surfaces of the side pod. Inspired by the bargeboards of actual Formula 1 cars, a turning vane was implemented. This successfully redirected airflow and reduced drag by 0.6%.



✦ Pathlines Analysis - Airflow being redirected outboard by turning vane. Credit: Hydron

A large volume of extra material is present in the side pod. By cutting away pockets, the centre of mass is aligned closer to the canister thrust vector. Through changing the thickness at the front or rear of the pocket, the centre of mass can be fine-tuned to be as far rearwards as possible while remaining stable when a canister is inserted. By determining the location of the centre of mass when changing parameters of these pockets, we could find the most suitable dimensions.

CENTRE OF MASS PLACEMENT			
FRONT WALL THICKNESS [mm]	REAR WALL THICKNESS [mm]	VERTICAL DISPLACEMENT FROM THRUST VECTOR [mm]	HORIZONTAL DISPLACEMENT FROM ORIGIN [mm]
NONE	NONE	7.1	71.6
2	2	4.47	72.9
2	4	4.55	72.85
2	6	4.6	72.78
2	8	4.74	72.0
4	2	4.52	72.2
4	4	4.64	72.18
4	6	4.73	72.15
4	8	4.82	71.3
6	2	4.61	71.4
6	4	4.7	71.45
6	6	4.83	71.5
6	8	4.92	71.5
8	2	4.8	71.7
8	4	4.81	71.65
8	6	4.85	71.6
8	8	4.95	71.6

## SIDE POD EVALUATION

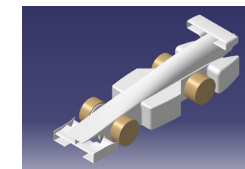
The final side pod design, the flat side pod design, was chosen as it achieved achieving the lowest drag value and was the easiest to manufacture. The final side pocket dimensions were chosen with an 8mm wall from the front to not only balance the centre of mass in front of the

rear wheel axle for stability, but also to act as a physical 'buffer' between the front face of the side pod, where the higher pressure air in front of the side pod could roll underneath the side pod and cause extra drag through eventual collision with the rotating surface of the rear wheel.

## REAR WING

### HORIZONTAL SUPPORTS

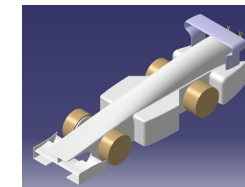
The position of the legal rear wing surface meant that there were several options for its support structure. The first design was a simple solution with minimal frontal area; horizontal supports which attached to the canister housing.



✦ Credit: Hydron

### VERTICAL SUPPORTS

While horizontal supports provided the minimum drag, vertical wing supports were also trialled, particularly for the yaw stability benefits of more vertical surfaces towards the rear of the car. When the restoring moment and drag forces of this design were input into our race model, the increased drag outweighed the stability benefits, so this design was no longer pursued.

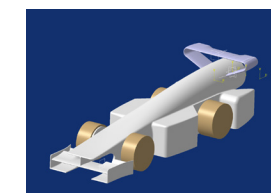
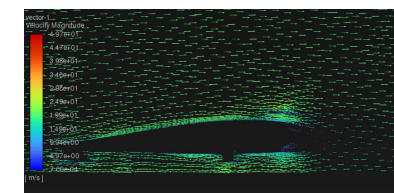


✦ Credit: Hydron

### TWISTED REAR WING/ADJUSTED ANGLE OF ATTACK

At the rear of the car the largest low pressure zone forms behind the canister, which is a large contributor to the pressure drag of a car. In an attempt to minimise the wake of the canister chamber, the rear wing was angled so that it deflected airflow towards the low pressure zone and minimised the drag produced by it. This idea had two implementations, the first with an asymmetrical aerofoil following the entire rear wing and support structure. The second implementation was more refined, inspired by the curved rear wings of Formula 1 cars, with a single portion of the rear wing angled.

Initially trialled on Prototype B, these designs yielded a lower drag force, but when introduced on our final prototype, drag was increased and thus this innovation was not included in our final design.



✦ Credit: Hydron

# FINAL CAR & DEVELOPMENT EVALUATION

## EVALUATION

- » Drag: 0.2542 [N]
- » Lift: -0.1896 [N]
- » Mathematical Model Race Time: 1.063 [s]

When viewing the performance of components holistically, each component was developed the most optimisation for their respective flow conditions.

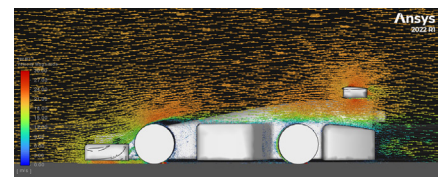
**Nosecone** - aiding to minimise the airflow redirected into the front wheel, the nosecone maintained our innovation from Nationals with a slight convex-outer edge transitioning to a slight concave profile in the middle of the nosecone to gently coerce airflow away from the front wheels.

**Front wing** - with the main purpose of redirecting airflow away from the surfaces of the front wheel, this resulted in design where a majority of the airflow was redirected to the top and side faces of the side pod as well as into the central channel.

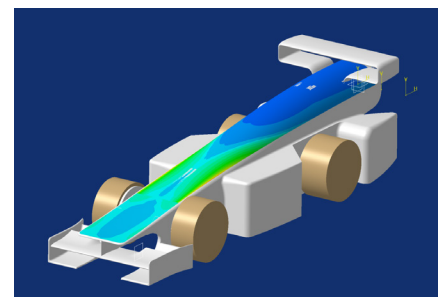
**Side pods** - accommodated for airflow redirection from front wing, with a slight angle to prevent collision the part's front face.

**Rear pod** - were fine-tuned to reduce the size of the separation zone behind the rear wheels as much as possible, utilising the coanda effect to connect airflow on either side of the component.

**Rear wing** - being one of the rearmost components of the design, it was developed to the most optimal configuration and shape. The thinner support reduces rear wing frontal area by 9.67% with minimal effect on the durability of the component, while fine-tuned to the most optimal height to aiding in airflow connection on the rear pod.



\* Vector Analysis - Airflow over the side components of the car, with good flow attachment. Credit: Hydron



\* Surface Curvature Analysis - Surface with continuous and gradually changing curvature. Credit: Hydron



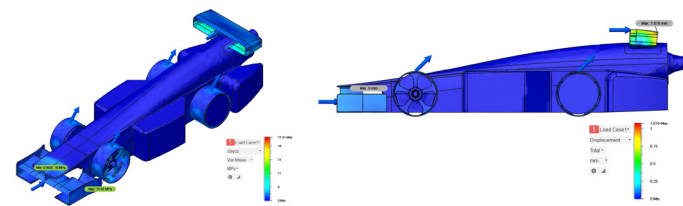
\* Isophotes Curvature Mapping - Tangent Surfaces with no sudden curvature changes. Credit: Hydron

## FEA TESTING

In order to confirm the structural integrity of the car, and that it could withstand 10 races, we ran a full car FEA simulation. During deceleration at the end of the track, the car experiences the highest forces, a total of approximately 4.5N.

We defined forces on all components of the car as if they were the sole component which the 4.5 N force acted on. To allow for a safety factor of approximately 2:1, we increased this force to 10N for each component.

From our first test, the maximum stress was found to be at the tether line guides. While the stress was high at 195.1 MPa, it was still within titanium's yield strength of 210 MPa and we were satisfied with using our chosen model of tether line guides.



\* FEA Test excluding tether line guides. Note: Front hubcap hidden to show internal wheel stress. Credit: Hydron

The simulation was repeated, this time without tether line guides in order to make other stresses more visible. The new peak stress occurred in the wheels, which at 27.81 MPa was well within the yield strengths of all chosen materials. Maximum displacement occurred in the rear wing at 1.076mm. While this was a large amount of displacement, plastic deformation still had not occurred and the test case was well beyond what the rear wing would actually experience. Therefore, we were confident that all of our components would be able to withstand the forces of racing, and settled on our final design.

## WIND TUNNEL TESTING

In order to validate our aerodynamic development of the car centred around CFD use, we tested our car in physical wind tunnels. This allowed us to record a real world drag force, as well as visualise flow in order to verify flow structures.

Using the drag measurements from the wind tunnel of 22g, which equates to 0.2159N, we concluded that our car performed slightly better than when simulated, with a difference of 0.02N in drag.

Using the drag measurements from the wind tunnel of 22g, which equates to 0.2159N, we concluded that our car performed slightly better than when simulated, with a difference of 0.02N in drag.



\* Final car airflow structure verification using smoke in wind tunnel. Credit: Hydron

Using a smoke machine and a low speed wind tunnel, we were able to visualise areas of flow detachment or turbulent flow, due to stationary or diffused smoke. As expected, flow detached around the exclusion zones of the wheels, but successfully reattached afterwards over the side and rear pods.

## WEIGHT DISTRIBUTION & CANISTER ANGLE

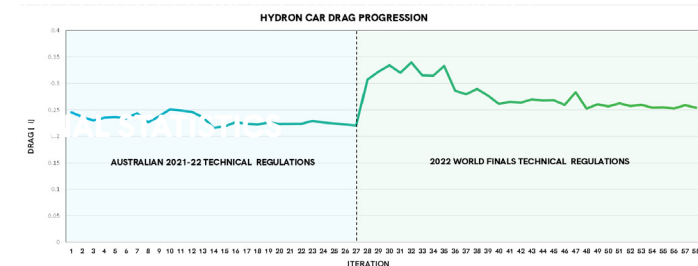
As the weight distribution of the car is integral to both minimise the tipping moment and the rate of yaw, further methods of controlling the location of the centre of mass were implemented on our final car. In addition to the weight distribution pockets in our side pods, we controlled the mass of the car through material selection for front and rear axles. Mild steel was used for the front wheels, and aluminium for the rear wheels, shifting the centre of mass marginally forward, in order to ensure that it was between the front and rear wheels, and the car was stable. These weight distribution techniques also allowed us to control the final mass of the car, remaining as close to 50 grams as possible. A final canister angle of 2 degrees was chosen, which in combination with our weight distribution pockets and axle choice, allowed us to bring the thrust vector within 5mm, satisfying our goal and ensuring that tipping was kept to a minimum.

## TETHER LINE GUIDES

For our final car, we selected Fuji Titanium Torzite Guides. The torzite ceramic inner ring has an extremely low coefficient of friction, of approximately 0.15. Alternative options such as a bare titanium ring or a Nylon 12 3D printed part have average coefficients of friction of 0.5 and 0.3 respectively. An increased coefficient of friction to 0.5 would have resulted in a race time of 1.099 seconds, adding 0.036 seconds to race times. Therefore Titanium Torzite was the best choice for our tether line guides.

## PART INTEGRATION

The many individually manufactured components of a car increase manufacturing complexity, resulting in higher chances of errors being made during assembly as well as increasing manufacturing time. For this reason we minimised the amount of individual components, utilising wheel support structures as additional support structures for tether line guides. This also had the benefit of ensuring that parts were structurally sound and not dependent on glue for their strength.



## FINAL STATISTICS

### Objectives

Through rigorous testing, research and ongoing evaluation, we developed a car which met the objectives which we determined as key indicators to a car's performance. With an overall decrease in drag from our first model to our final model of 17.95%, we were able to

### Aerodynamics

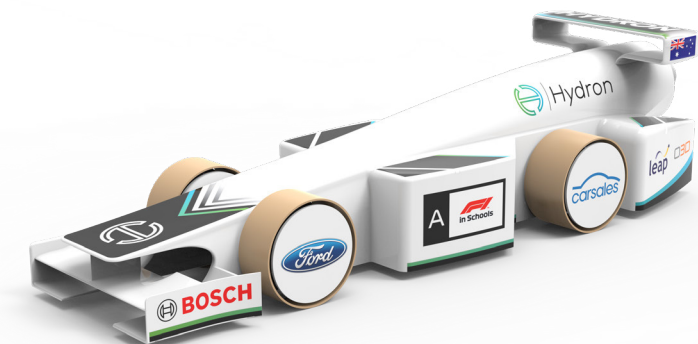
The final car met the aerodynamic design objectives we sought to achieve, with a design focussed on redirecting air away from the rotating wheel surfaces. As a result, our car achieved a drag force of 0.2542N.

### Durability

Through FEA simulations completed in Autodesk Fusion 360, all components were ensured to be sufficiently durable.

### Mass

Through the inclusion of weight-reduction pockets, thin chamber walls, and carefully selecting component materials with high strength yet low densities, the overall mass of the car was kept as low as possible for manufacturing.



## SOFTWARE CHOICE

### CATIA V5

CATIA v5 was our main CAD software used to design the car. CATIA v5 offers controlled, precise development over specific surfaces with its different workbenches, and a tree navigation system which can be used to view exactly which commands and body are influenced by a command, showing the parents/children of any command. This navigation system enables easy problem solving in the event that a change in a parent results in errors in children commands.

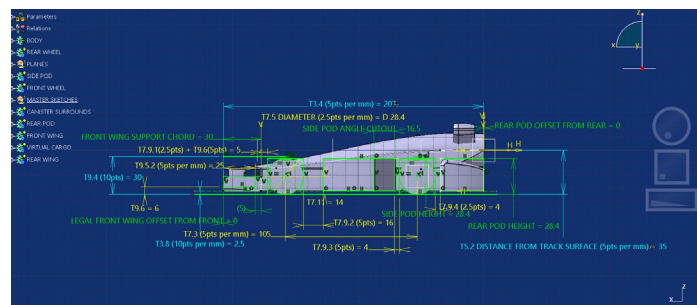
### AUTODESK FUSION 360

Fusion 360 was another software used by our team to further streamline the design process. Fusion 360 enabled rapid editing of the 3D model, therefore making it suitable for preparing models for manufacturing or for FEA, where quick iterative design changes to a component can be made.

## CAD ORGANISATION

### MASTER SKETCHES

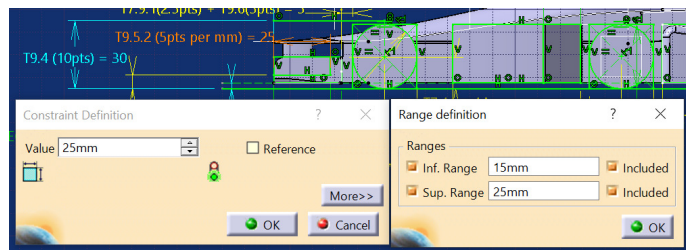
A master sketch is created to control the dimensions of side components, with each feature designed to conform to the parameters assigned to it. This allows the length of components to be easily changed while testing models, simply by editing this one sketch. Parameters are able to be edited externally through the tree navigation, enabling an easy change to any defined parameter.



\* CATIA v5: Master Sketch constraining side components. Credit: Hydron

### LABELLING & LIMITING DIMENSIONS

To ensure compliance with regulations, key dimensions were labelled for their respective regulation in the master sketch. To prevent accidentally changing parameters to infringe a regulation when making edits, limits were added to dimensions, which ensured parameters were only accepted if the input resulted in legal component dimensions.



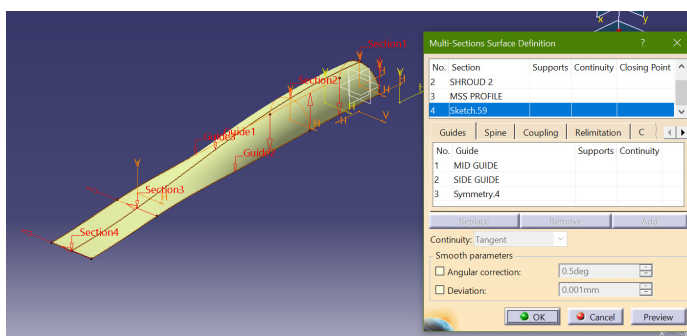
\* CATIA v5: A limited dimension, ensuring that the front wing remains in a legal location. Credit: Hydron

## SURFACE MODELLING

In order to design a car as aerodynamically efficient as possible, streamlined complex geometry was required in many parts of the car, such as the main body and front wing. Geometrically simple components could be easily modelled using the Part Design workbench of CATIA with commands such as pads, shells and fillets. For more complex geometry, the Generative Shape Design workbench was used, allowing finer control and more intricate aerodynamic surfaces to be modelled.

### MULTI-SELECTION SURFACE

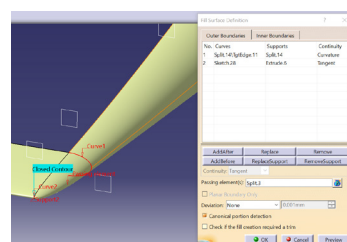
In order to model the main body of all prototypes including our final car, the Multi Section Surface tool was used. Multiple profiles were created, connected by guides which constrained the geometry. Other constraints such as tangencies with other surfaces were also used in order to create smooth connections between parts. These guides, profiles and tangencies allowed us to accurately control the surfaces, while maintaining shapes which resulted in a gradual pressure gradient along their lengths, reducing pressure drag and airflow separation.



\* CATIA v5: A Multi-Sections Surface used to form the primary surface of a main body. Credit: Hydron

### FILL

While not used in our final car, fills played an important role in producing aerodynamic surfaces such as the nosecone of prototype 2. Fills can be defined by a



\* CATIA v5: A fill surface with tangency constraints ensuring a smooth attachment to other surfaces. Credit: Hydron

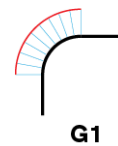
boundary, tangency conditions with other surfaces, and passing elements, which allows a high level of control of the resultant surface.

## SURFACE CONTINUITY

The concept and levels of surface continuity were investigated as we aimed for our aerodynamic surfaces to be smooth and result in an even pressure gradient.



**G0 continuity** means that two surfaces meet each other along an edge, and was a level of continuity necessary to produce a manufacturable car.



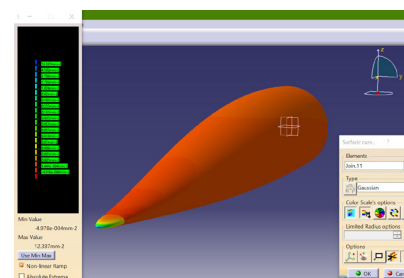
**G1 continuity** means that two surfaces are tangent at their joining edge, and was a level of continuity identified as the minimum across all of our aerodynamic surfaces. G1 continuity was achieved through fillets and tangency constraints on complex surfaces.



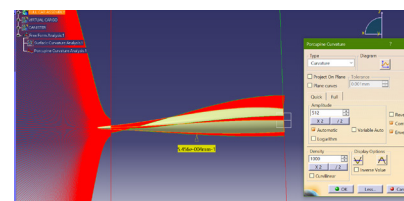
**G2 continuity** means that two surfaces have equal curvature at their joining edge, and was explored as an option for critical joints, such as between the nosecone and main body of prototype 2. While it did result in a smoother surface than G1 continuity, G2 continuity was deemed unnecessary due to its difficulty to properly constrain and implement in designs.

\* Credit: Hydron

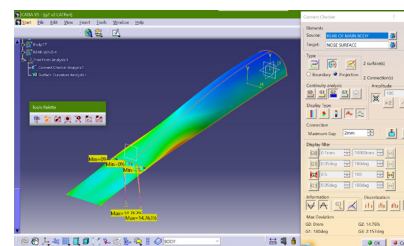
Following this investigation, G1 continuity was identified as the level of continuity to be implemented across all aerodynamic components of our car.



\* CATIA v5: Surface Curvature Analysis - Gaussian Curvature analysis of two G1 continuous surfaces, highlighting unmatched curvature. Credit: Hydron



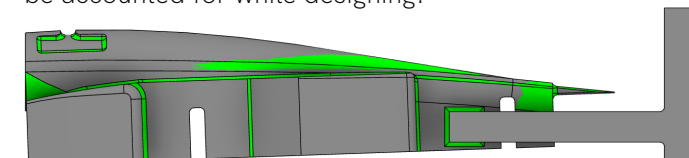
\* CATIA v5: Porcupine Curvature Analysis - Discontinuous curvature, G1 continuity. Credit: Hydron



\* CATIA v5: Connect Checker - G2 continuity with a maximum deviation of 14.76%, while Gaussian curvature shows more matched curvature than G1. Credit: Hydron

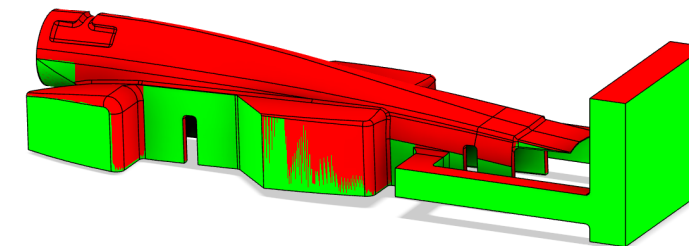
## PREPARATION FOR MANUFACTURING

As the main body of our car was CNC machined, the car geometry needed to account for the limitations of such a process. Limitations of CNC milling include the inability to cut internal sharp edges without fillets, due to the radius of endmills. A 3mm diameter ball nose endmill was selected to minimise this limitation, but it still needed to be accounted for while designing.

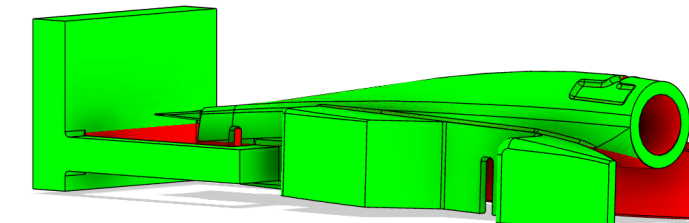


\* Fusion 360: Minimum Radius Analysis of 1.5mm, ensuring that all concave parts of the car would be accessible to a 3mm ball nose endmill. Credit: Hydron

CNC mills are also unable to create geometry with undercuts, or surfaces which are hidden by other parts of the workpiece when viewed from the tool's perspective. The Minimum Radius Analysis and Accessibility Analysis tools in Fusion 360 were used to ensure that the car was manufacturable, and helped determine what cuts would be necessary to fully machine our car.



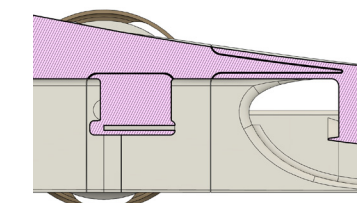
\* Fusion 360: Accessibility Analysis from below, showing side pod surfaces are not fully accessible due to the angle of the workpiece. Credit: Hydron



\* Fusion 360: Accessibility Analysis In combination with a side milling operation, the side pod surface and the whole side of the car could be milled properly. Credit: Hydron

## OFFSET SPLIT SURFACES

Rather than splitting components from a single surface, 2 surfaces with a 0.1mm offset were used as splitting tools. This resulted in a 0.1mm gap between parts, allowing space for gluing and reducing hand sanding to achieve a good fit between parts.



\* Fusion 360: Section Analysis of joints between foam body and nosecone, as well as joint between foam body and front wheel support, all with 0.1mm gap. Credit: Hydron

## MACHINING GOALS

When manufacturing our cars, we defined several goals in order to efficiently produce high-quality cars.

- » Accurately produce 2 race cars with maximum tolerances of  $\pm 0.1$ mm from CAD model.
- » Produce cars that are compliant with all regulations.
- » Produce cars with masses as close to 50 grams as possible while allowing tolerances for scrutineering.
- » Minimise hand finishing.

## CNC EQUIPMENT

When manufacturing our cars, we utilized our school's in-house Denford 6600 Pro CNC router. The large cutting bed volume of 1000 x 600 x 110 millimetres in conjunction with its 4-axis machining capabilities made it the ideal option for producing our cars with speed, precision and efficiency. This model also provides a great deal of control over the spindle, with a customizable feed rate and spindle speed.

Specifically, there is a maximum spindle speed of 2400 RPM, and a minimum feed rate of 5000 millimetres per minute. The machine utilizes stepper motors for axes control. We decided to take advantage of the precision of the CNC milling machine by using a 3 millimetre ball nose cutter for all final machining plans. Additionally, a rotary fixture allowed the router to mill on multiple axes which shared a cutter, without requiring manual interaction.



» Our school's Denford 6600 Pro CNC Router. Credit: Hydron

## MACHINING TOLERANCE

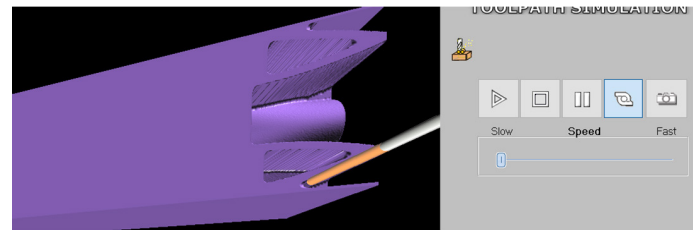
When developing cars, a standard tolerance was used for parts to ensure the highest quality with minimal hand finishing. Using a standard tolerance grade of IT12 in the dimensions applied in our CAD models created a precise fit for components while also providing leeway for manufacturing error. This tolerance grade has a minimum of 0.1mm clearance and a typical maximum of 0.2mm, depending on the nominal size of the component connection.

Different tolerances were applied for specific areas of the car, such as in areas where paint build-up can result in the infringement of regulations. As a result, in regions pertaining to exclusion zones, namely those of the wheel

exclusion zones, a tolerance of 1mm was implemented to account for additive processes during manufacturing.

While the CNC milling machine has tolerances of  $\pm 0.1$ mm, this tolerance changes with the expansion of the CNC machine due to heat. For this reason, we aimed to keep our total CNC milling plans as short as possible, minimising heating and thus tolerance creep.

As the official F1 model block foam is inherently flexible, especially in thin parts, our machining plans started furthest from the support and milled towards it, ensuring that the section being cut was as supported and rigid as possible, minimising dimensional inaccuracies.



» Final machining plan starting furthest from support structure on underside. Credit: Hydron



» Machining from the rear of the car towards the front on original machining plan. Credit: Hydron

Due to these sources of inaccuracies in milling, we added a 0.2mm finishing amount. The amount of 0.2mm was chosen as it meant that even at maximum deviation, the machine would not mill out more than the original design. 0.2mm was also a sufficiently low amount to result in minimal hand sanding and finishing.

## MACHINING PLANS

We tested our initial machining plan on a balsa block in order to evaluate the quality and rectify any issues without wasting any foam blocks. After comparing this milled car with the CAD model, we identified few dimensional errors, but noted an inaccuracy of 0.15mm at the nosecone connection, as well as several surface finish issues, such as ridges between machining zones.



» Test balsa milled car, with machining errors on sidepod and in central tunnel. Credit: Hydron

Following this model we significantly altered our machining approach. This initial approach used both 3mm and 6mm ball nose endmills, and 5 bottom machining plans, 2 top machining plans, and 4 side machining plans.

Our new approach was simpler and shorter, reducing tolerance creep and ridges between machining zones. The finishing amount was also added during this stage, to account for any remaining inaccuracies.

The new machining plan consisted of 1 bottom machining plan with 2 passes and 2 side machining plans, with 2 passes each, all using a 3mm ball nose bit. This was significantly faster and resulted in a milled car without any defects.



» Car milled from foam block using new machining plan, without defects. Credit: Hydron

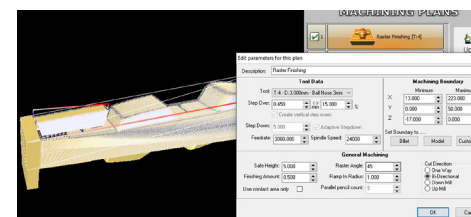
## COMPUTER AIDED MANUFACTURING (CAM)

### CAM SOFTWARE

CAM software is extremely important when using machine tools, and in this case, was responsible for the creation of G-Code for our CNC router. We opted to use Quick Cam Pro when carrying out this process for the World Finals; a selection made due to the software's native integration with Denford routers, simplistic user interface and comprehensive machining plans, as well as our team having experience with this software in past competitions. On top of this, Quick Cam Pro allowed us to adjust machining boundaries, step over, feed rate, spindle rate, safe height, overall tolerance, raster angle, cut width, cut depth, as well as tool type. These features of the software provided us excellent control, allowing us to utilise the router to its full potential.

### CAM SETTINGS

Establishing parameters for the numerous variables of CAM manufacturing is crucial to achieving a successful process. Each of our values have been refined through previous competitions, and as such we have reached a standard that produces consistent, high-quality finishes. Specifically, these parameters were as follows: 0.45mm 15% step over, 3000 mm/s feed rate, 24000 RPM spindle speed, 5mm safe height, 45 degree raster angle and bi-directional cut direction. The cutting tool parameter used was 3mm ball nose for all cuts.



» CAM settings for side machining plan. Credit: Hydron

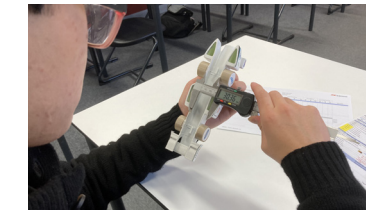
## QUALITY CONTROL

### COMPLIANCE

The most fundamental guidelines for car design are the regulations, which account for a large proportion of the overall score and determine whether or not a car is legal for the competition. We developed a system of two person checking and logging weights and critical dimensions during every stage of manufacturing, increasing the likelihood of any defects being detected, and consequently rectified.

Two full car scrutineering sessions were performed, one on the CAD model and one on the physical product. Aside from providing proof of legality, the physical scrutineering session provided insight into areas for future potential improvement, by comparing it to the initial digital scrutineering, representing manufacturing tolerance and quality.

Each car was weighed after each stage of the manufacturing process, ensuring that each car would be as close to 50.2g as possible when manufacturing was complete. This was especially important given that our race model attributed 41.65% of the car's performance to its mass. A mass of 50.2g was chosen in order to allow tolerance for any changes in moisture content, as well as for any weighing errors during scrutineering. Other critical dimensions were also recorded, to ensure no regulations were broken and no penalties would be incurred.



» A scrutineering session being conducted. Credit: Hydron

### GENERAL

In order to produce the highest quality cars at the end of the manufacturing process, we implemented the following further quality control strategies.

Rather than manufacturing only the necessary two race cars, we manufactured 6 cars. While we aimed to have tight tolerances with a maximum of 0.1mm deviation, some variation is inevitable. Manufacturing 6 cars meant that outliers which did not satisfy the tight tolerances could be rejected, with only the best two cars with the tightest tolerances being used as our race cars.

We employed the same process with our wheels, measuring bearing performance in addition to tolerances. We used our bearing test rig to burnish our bearings for 40,000 revolutions and then measured the final spin time from 12,000 rpm. Wheels were ranked and then grouped into full car sets.

Once we had selected our race cars, we fitted the best two sets of wheels to them, resulting in the overall highest quality cars.

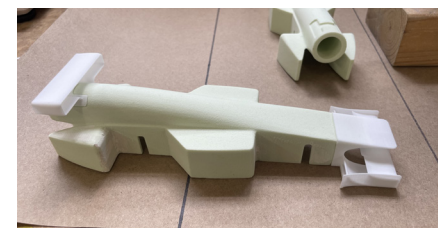
**MANUFACTURING PROCESS**

**SANDING & SEALING**

Following the CNC milling of the car, the support structure was sawn away. The car was then given a light sanding, starting with 360 grit sandpaper and moving to 400 grit to finish. Sanding removed scalloping and other surface defects, as well as the 0.2mm finishing amount, making the car dimensionally accurate to the CAD model. An unsealed official F1 Model Block foam is able to absorb moisture from the atmosphere, meaning that its weight can fluctuate with different humidity levels. In order to eliminate this inconsistency as well as bind the foam cells together, the sanded car was sealed with a mixture of equal parts PVA and water.

**ASSEMBLY**

Before the assembly of our nylon 12 parts and foam body, a dry run was conducted to ensure that the fit was adequate. In order to properly align all components of the car while gluing, particularly the wheel support structures, an assembly jig was used (see Assembly Jig). After a successful dry fit, 5 minute epoxy was used to glue the parts together. The glued car was left in the alignment jig to cure for at least 1 hour to ensure that alignment was maintained.



\* An assembled and glued car. Credit: Hydron

**PUTTYING**

Wood putty was used to fill in any grooves or gouges on the foam body as well as any gaps such as those between the nosecone and foam body. The putty was left to dry, and then sanded back so that the surface was smooth and consistent with the rest of the car.

**PRIMER**

Three coats of primer were applied to each of the cars, followed by a light 400 grit sanding after each coat had dried. This resulted in an extremely smooth surface, which was a high quality base for the final coats of paint, critical for a good surface finish.

**FINISHING**

After all coats of primer were completed and the cars were dry, 1 to 2 coats of white automotive paint were then applied to the car. Most cars received a single

coat of white paint, but those which were significantly underweight or had visual defects were given a second coat. Once the paint was dry, waterslide decals were applied, forming our livery and sponsor placement on the car. 1 to 3 coats of clear coat were then applied to secure the decals in place, and give the car a gloss surface finish. If a car was still underweight following the first coat of clear coat, additional coats were applied until the car was of a satisfactory weight.



\* All 6 cars drying after a coat of white automotive paint. Credit: Hydron

**ASSEMBLY JIG**

To ensure consistency when gluing components of the car together, an assembly jig was used. This assembly jig featured a sliding piece with a negative impression of the leading features to align the nosecone. This was crucial for not only quality control between cars, but also in ensuring aerodynamic stability for the car - a slightly angled nosecone would result in aerodynamic yaw to one side of the car. The jig was manufactured using FDM PLA plastic, with tolerances within 0.1mm of the nominal sizes shown within the CAD model. However, issues arose in the axle alignment holes, where the bridging led to inconsistent shrinkage between different holes. As a result, the alignment holes were edited in the CAD model which was reprinted, meaning that the holes could then be used accurately. The quality of the assembly jig was also consolidated by attaching it to a flat melamine particleboard sheet, ensuring that there were no bends or inaccuracies in the assembly jig itself.



\* Assembly Jig with alignment axles inserted. Credit: Hydron

**OUTSOURCING**

**NYLON PARTS**

Our team outsourced to Objective 3D for access to a wider range of possible 3D printing methods. Of the 3D printing methods available, SLS (Selective Laser Sintering) was determined to be optimal, due to tight tolerances of  $\pm 0.1$ mm, design freedom and available materials. The process of SLS 3D printing involves the sintering of thin

layers of powdered plastic, which allows intricate details to be manufactured without support material, and results in parts without layer line defects. Nylon 12, an available SLS material has a sufficiently high yield strength of 53MPa and is able to elastically deform before breaking, making it ideal for our application. SLS 3D printing also yields high strength parts, with similar strengths to those of injection moulded parts.

All of these properties made SLS 3D printing far superior to FDM (Fused Deposition Modelling) 3D printing components, which would have been the only option without outsourcing.

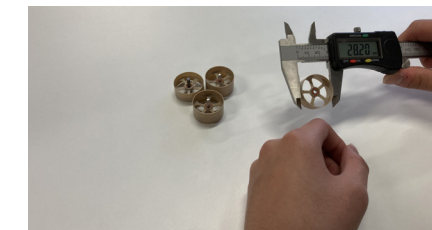


\* Nylon 12 parts from Objective 3D. Credit: Hydron

**PEEK WHEELS**

Our team outsourced our wheels to ArpTech for tight tolerance CNC machining, and use of a CNC lathe. ArpTech were able to manufacture our wheels to  $\pm 0.05$ mm tolerances allowing us to further reduce the diameter of our wheels, which would have been impossible to achieve without outsourcing.

Using a CNC lathe allowed us to ensure that our wheels were circular and concentric, critical to reducing rolling resistance and achieving fast lap times. CNC machining our wheels also allowed us to use advanced engineering plastics, such as PEEK, which cannot be 3D printed and which has ideal properties for our wheels.



\* Checking dimensions of PEEK wheels from ArpTech, measuring a 28.2mm diameter exactly as designed. Credit: Hydron

**WORKPLACE SAFETY**

In order to ensure that our manufacturing process was as safe as possible a risk assessment was undertaken and risk control procedures were enacted.

RISK DESCRIPTION:	CAUSES OF RISK:	PROBABILITY:	IMPACT:	RISK SCORE (PROBABILITY X IMPACT):	RISK CONTROL:
Skin, Eye and Lung Irritation	Foam dust exposure and inhalation	0.6	0.4	0.24	A dust collection system was used in the CNC router, minimising loose dust after CNC machining was complete. Hand sanding of cars was conducted in a well ventilated area.
Drowsiness or dizziness	Prolonged aerosol spray paint inhalation	0.4	0.6	0.24	All spray painting was conducted outdoors with good ventilation. PPE in the form of a dust mask was worn during painting.
Entanglement or impact	Operator entanglement in CNC router, or CNC router ejecting workpiece	0.1	0.8	0.08	All CNC milling operations were conducted under the supervision of an experienced teacher. The workpiece was checked to be firmly secured and the safety door was closed before all cuts. Loose clothing was restricted with a dust coat.
Cuts and lacerations	Using Junior Hacksaw to remove support material from CNC milled parts	0.1	0.2	0.02	The workpiece was securely held, and it was ensured that fingers were away from the cutting path.

Specific and pertinent information on material hazards was gained through referring to Safety Data Sheets, primarily for items such as the primer we used. These sheets helped us to identify ways to mitigate risks such as protecting primer from direct sunlight or heat. In addition, Safety Data Sheets informed us on first aid procedures if any emergencies related to the materials eventuated.